ELSEVIER

Earth and Planetary Science Letters 164 (1998) 277–284

EPSL

The depth of the spinel to garnet transition at the peridotite solidus

J. Andrew C. Robinson, Bernard J. Wood *

CETSEI, Department of Earth Sciences, University of Bristol, Wills Memorial Building, Bristol, BS8 1RJ, UK

Received 2 March 1998; revised version received 28 September 1998; accepted 28 September 1998

Abstract

We have determined the pressure and temperature of the spinel–garnet transition close to the solidus of fertile and depleted peridotite from a combination of synthesis, sandwich and garnet-seeded experiments. Garnet is unstable in MORB-Pyrolite below 2.8 GPa (depths <85 km) at a solidus temperature of 1470ºC. In Tinaquillo Lherzolite, which is related to MORB-Pyrolite by about 7% fractional melting, the transformation occurs at 3.1 GPa at a solidus temperature of 1520ºC. In both cases the transformation interval is narrow, approximately 0.1–0.2 GPa. Because the solidus temperature increases by 7ºC and the spinel–garnet transformation pressure by 0.05 GPa for every 1% melt extracted, extremely high potential temperatures (T_p > 1450ºC) are required to generate the 3–5% melting in the garnet field implied by recent trace element and isotope studies. It appears likely, therefore, that the 'garnet signature' arises from some mechanism other than anhydrous melting of garnet peridotite. © 1998 Elsevier Science B.V. All rights reserved.

Keywords: peridotites; spinel; garnet group; lherzolite; pyrolite

1. Introduction

The chemical and isotopic compositions of mid-ocean ridge basalts (MORB) are frequently inferred to indicate that, beneath ridges, melting of the mantle begins in the stability field of garnet peridotite [1–5]. This conclusion is based on excesses of ^{230}Th over its parent ^{238}U [2,4,6], on enrichments in Hf relative to Lu [1,5] and on the general REE pattern of MORB glasses [3]. It places important constraints on the temperature of adiabatically upwelling mantle since partial fusion of garnet peridotite requires higher potential temperatures and generates greater thicknesses of oceanic crust, than does melting of its low-pressure equivalent, spinel peridotite [3,7,8].

Despite its importance, however, there are few good experimental constraints on the pressure and temperature of the spinel–garnet transition at the solidus of mantle peridotite. Most data are either widely spaced in pressure and unreversed [9–13], or were obtained on simple model systems [14–16], or were obtained at temperatures well below the solidus [14–16]. Lack of accurate data has resulted in the adoption, in modelling studies, of a range of *P–T* properties for the spinel–garnet transition. Garnet is frequently assumed to begin breaking down to spinel at about 80 km depth (2.7 GPa) with the transformation taking place over an interval down to 60 km (2.0 GPa) at which point garnet disappears [3,17]. A cursory examination of the available experimental data (e.g. [9]) suggests, however, that garnet is actually limited to depths greater than 80 km. If correct, the restriction of garnet stability to high pressure means

* Corresponding author. Fax: +44 117 9253 385; E-mail: b.j.wood@bristol.ac.uk

0012-821X/98/$ – see front matter © 1998 Elsevier Science B.V. All rights reserved.
PII: S0012-821X(98)00213-1

that potential temperatures required to generate melting in the garnet field should produce much greater thicknesses of oceanic crust than are generally observed [18]. In that case the so-called 'garnet-signature' would require an alternative explanation, such as lower pressure melting of veins of garnet pyroxenite [19], or a change in the trace element partitioning behaviour of clinopyroxene above 1.5 GPa [20].

In view of its importance we have determined the pressure of the spinel–garnet transformation in fertile (MORB-Pyrolite) and depleted peridotite (Tinaquillo Lherzolite) at temperatures close to the solidus. The data place firm constraints on the depth of origin of basaltic rocks which exhibit systematic geochemical evidence for garnet having been a residual phase during their genesis.

2. Method

The two starting compositions, MORB-Pyrolite and Tinaquillo Lherzolite (Table 1) were sintered oxide mixes prepared and reduced using procedures described in an earlier paper [21]. Experiments were performed in graphite inner capsules loaded into 3 mm O.D. platinum capsules and welded shut. A combination of techniques ensure near-anhydrous conditions [21] and we have found from FTIR measurements that product glasses synthesized at 1.5 GPa for 24 h contain <0.1wt% H_2O. Given the reduced nature of the starting materials, which were sintered at an f_{O_2} two log units below the fayalite–magnetite–quartz (FMQ) buffer [21], little or no CO_2 should be present in the experiments. Experiments were performed in a 1/2-inch piston cylinder apparatus using the hot piston-out technique [22] with a single sleeve of CaF_2 as the pressure medium and crushable alumina as the inner spacers. Pressure calibrations, based on the melting point of gold [23] and on the albite–jadeite–quartz reaction [24] result in a -7% pressure correction for this assembly and pressurisation method. Pressure reproducibility is approximately ± 0.05 Gpa. Experimental temperature was monitored and controlled to within 1ºC using a WRe3/WRe25 (D-type) thermocouple situated on top of the capsule and protected from it using a thin (1 mm) alumina disc. Reported temperatures are corrected for a small (3ºC/mm) gradient in the hot zone of the furnace [21]. Based on reproducibility of liquid compositions at 1.5 GPa we estimate a temperature precision of ± 10–15ºC.

The experiments were of four kinds.

(1) *Direct experiments* involved holding the bulk composition (MORB-Pyrolite or Tinaquillo Lherzolite) at just above its estimated solidus. The relative volumes of crystals and quenched melt in experiments 140 and 141 were then determined from high-contrast back-scattered electron micrographs using NIH-IMAGE software. We found that both the Fe-rich quenched melt and the quench overgrowths on stable crystals are clearly distinguishable using this approach. In each case, analyses of three different slices through the same capsule gave agreement in melt fraction to within ± 0.3% absolute. In other experiments the fraction of melt was estimated by visual comparison of electron micrographs with those of experiments 140 and 141. Although the absolute melt fraction is not important in the determination of the solidus temperature, back-scattered electron micrographs enable detection of trace amounts of melt (Table 2) which indicate that the solidus has been crossed.

(2) *Sandwich experiments*. Approximately 20% of a basalt close to equilibrium with the residue is

Table 1
Starting compositions

	SiO_2	TiO_2	Al_2O_3	FeO	MgO	CaO	Na_2O	Cr_2O_3
MPY	44.7	0.17	4.37	7.55	38.6	3.38	0.40	0.45
Tinaquillo	44.9	0.08	3.22	7.58	40.0	2.99	0.18	0.28
#82	47.8	1.09	14.9	6.26	16.5	9.11	4.20	0.17
#84	50.9	1.49	17.1	6.33	10.0	6.97	7.23	0.02

Synthesis of the starting compositions is described in the text and in Ref. [21]. Note that Tinaquillo Lherzolite composition is slightly lower in Cr_2O_3 than that of Ref. [25].

Table 2
Experimental conditions

Run No.	*P* (GPa)	*T* (ºC)	Duration (h)	Peridotite	Run type [a]	Basalt (wt.%)	Basalt	F (vol.%) [b]	Phases present [c]
121	2.7	1448	26	MPY	Micro	6	#82	tr	Ol, Opx, Cpx, Sp, L
136	2.7	1471	24	MPY	Direct	–	–	2–5	Ol, Opx, Cpx, Sp(tr), L
140	2.7	1483	27	MPY	Gt-seeded	–	–	7	Ol, Opx, Cpx, Sp(tr), L
122	2.8	1478	25	MPY	Micro	2.5	#84	<10	Ol, Opx, Cpx, Sp(tr), Gt, L
117	3.0	1468	26	MPY	Micro	20.5	#82	tr	Ol, Opx(tr), Cpx, Sp(tr), Gt, L
116	3.0	1488	27	MPY	Micro	<5	#82	3–8	Ol, Opx, Cpx, Sp(tr), Gt, L
88	3.0	1507	16	T.L.	Sandwich	18	#4	Sub-solidus	Ol, Opx, Cpx, Sp
134	3.0	1528	29	T.L.	Micro	8	#82	≈10	Ol, Opx, Cpx, L
120	3.0	1531	34	T.L.	Micro	10	#82	≈10	Ol, Opx, Cpx, L
93	3.0	1550	16	T.L.	Sandwich	27	#3		Ol, Opx, L
142	3.1	1521	6	T.L.	Gt-seeded	–	–	tr	Ol, Opx, Cpx, Sp(tr), L
144	3.1	1521	13	T.L.	Gt-seeded	–	–	tr	Ol, Opx, Cpx, Gt, L
141	3.2	1533	28	T.L.	Gt-seeded	–	–	4	Ol, Opx, Cpx, Gt, L
138	3.2	1553	28	T.L.	Direct	–	–	10–15	Ol, Opx, L
129	3.3	1538	24	T.L.	Micro	13	#82	<5	Ol, Opx, Cpx, Gt, L

[a] *Micro* is a variation on the sandwich technique [21] which utilises 70–100 μm diameter vitreous carbon spheres to minimise quench modification of the liquid by acting as a baffle at the crystal–liquid interface. *Direct* employs no basaltic component at the start of the experiment. *Gt-seeded* uses a mixture of garnet peridotite and sintered oxide mix without added basalt. *Sandwich* is a standard sandwich experiment [21].

[b] The melt fractions in experiments 140 and 141 were determined by image analysis of back-scattered electron micrographs. In each case three separate slices were analysed and a total deviation of ±0.3% was obtained. Melt fractions in other experiments are estimates based on electron micrographs which were visually compared with those of 140 and 141.

[c] Ol, olivine; Opx, orthopyroxene; Cpx, clinopyroxene; Sp, spinel; Gt, garnet; L, glass; (tr), trace amount.

added to the peridotite. The initial basalt compositions, #82 and #84 of Table 1, were derived by reacting a near-solidus liquid from 1.5 GPa ([21]) with MORB-Pyrolite at 3 GPa/1490º and 3 Gpa/1470º, respectively. Although melt fractions cannot, in this case, be used as indicators of solidus temperature, we have found, from mass-balance, that this method facilitates determination of the solidus temperature of the peridotite layer [21].

(3) *Micro-sandwich experiments*. A much smaller proportion of basalt than in (2) (normally <10%), is placed in the sandwich and separated from the peridotite part by a thin layer of vitreous carbon spheres [26]. The latter, the pores of which fill with melt during the experiment, were intended to act as an inhibitor to quench modification by minimising crystal growth at the basalt–peridotite interface. In fact, we find at pressures near 3 GPa that quench-modification is pervasive, even when the vitreous carbon layer is present. Electron micrographs of the peridotite part of the charge enabled estimation of melt fraction in the same way as for the direct experiments (Table 2).

(4) *Garnet-seeded experiments* started with a mixture of sintered oxide mix and the high pressure garnet lherzolite assemblage. The latter was synthesized by loading the reactive oxide starting mixes in graphite capsules and holding them at 3.5 GPa and 1400ºC for 22 h. Electron microprobe analysis confirmed that the correct assemblage was produced.

All analytical procedures are as reported in [21].

Experimental conditions and phases produced are given in Table 2. Compositions of all solid phases, with uncertainties, are presented in Table 3.

3. Results

Under conditions close to the peridotite solidus, the low pressure breakdown of garnet may be represented schematically as:

$$\text{spinel} + \text{orthopyroxene} + \text{clinopyroxene} = \text{garnet} + \text{olivine} \quad (1)$$

In a system of more than five components, such as mantle peridotite, garnet and spinel must, as al-

Table 3
Selected experimental phase compositions

Run No.	Phase [a]	No. [b]	Na_2O	MgO	Al_2O_3	SiO_2	CaO	TiO_2	FeO	Cr_2O_3	Mg#	
121	ol	12	0.03 (3)	48.8 (2)	0.20 (12)	40.7 (0)	0.31 (5)	0.01 (1)	9.74 (19)	0.24 (7)	0.90	101.3
(2.7 GPa)	opx (rim)	9 (48)	0.23 (2)	30.1 (1)	8.45 (16)	52.4 (1)	2.14 (5)	0.27 (1)	5.65 (13)	0.85 (5)	0.90	101.0
	cpx (av.)	147	0.90 (8)	22.8 (12)	8.07 (93)	52.1 (12)	10.1 (10)	0.38 (7)	4.81 (24)	0.84 (13)	0.89	100.4
	cpx (rim)	23	0.93 (4)	21.8 (2)	8.63 (24)	51.5 (2)	11.2 (1)	0.41 (3)	4.61 (15)	0.89 (9)	0.89	100.5
	spin	6	0.01 (1)	22.6 (2)	59.7 (2)	0.55 (61)	0.04 (2)	0.31 (2)	7.89 (12)	8.96 (56)	0.84	99.3
136	ol	24	0.03 (2)	49.2 (2)	0.22 (3)	40.6 (2)	0.31 (2)	0.02 (1)	9.32 (18)	0.28 (7)	0.90	101.2
(2.7 GPa)	opx (av.)	14	0.27 (10)	29.7 (15)	8.22 (165)	52.3 (12)	2.72 (76)	0.24 (14)	5.66 (26)	0.82 (17)	0.90	100.8
	cpx (av.)	58	0.77 (10)	23.7 (12)	7.96 (128)	52.0 (10)	9.41 (105)	0.29 (5)	5.03 (25)	0.88 (16)	0.89	100.9
	cpx (rim)	19	0.77 (4)	22.9 (2)	8.44 (12)	51.5 (2)	10.3 (2)	0.29 (2)	4.86 (13)	0.99 (9)	0.89	100.8
140	ol	44	0.04 (2)	49.5 (2)	0.20 (3)	40.9 (2)	0.34 (3)	0.00 (1)	8.82 (20)	0.26 (7)	0.91	100.8
(2.7 GPa)	opx (av.)	14	0.18 (6)	30.4 (6)	7.34 (60)	53.1 (4)	2.66 (38)	0.14 (8)	5.34 (14)	0.89 (10)	0.91	100.5
	cpx (av.)	46	0.54 (4)	23.9 (5)	7.71 (50)	52.2 (4)	9.71 (48)	0.18 (6)	4.78 (20)	1.00 (11)	0.90	100.5
122	ol	40	0.01 (1)	49.4 (2)	0.17 (3)	40.9 (2)	0.26 (2)	0.01 (1)	9.10 (23)	0.18 (5)	0.91	100.6
(2.8 GPa)	opx (av.)	20	0.24 (6)	29.8 (10)	8.48 (191)	52.5 (13)	2.40 (32)	0.15 (4)	5.36 (18)	1.09 (11)	0.91	100.5
	cpx (av.)	24	0.95 (11)	23.0 (3)	8.08 (140)	52.4 (10)	9.55 (61)	0.20 (3)	4.72 (19)	1.11 (14)	0.90	100.3
	gnt	40	0.00 (1)	22.1 (1)	22.3 (2)	42.3 (2)	5.16 (11)	0.37 (2)	5.63 (15)	2.23 (21)	0.87	101.2
117	ol	59	0.08 (4)	49.3 (2)	0.21 (4)	40.6 (2)	0.26 (2)	0.02 (2)	9.37 (20)	0.22 (6)	0.90	100.5
(3.0 GPa)	cpx (av.)	44	1.22 (26)	23.6 (18)	8.91 (179)	52.0 (12)	8.17 (156)	0.42 (7)	4.91 (27)	0.77 (12)	0.90	100.3
	cpx (rim)	28	1.36 (6)	22.9 (3)	8.81 (52)	52.0 (3)	8.95 (27)	0.43 (4)	4.76 (16)	0.80 (10)	0.90	100.3
	gnt	5	0.08 (4)	22.2 (4)	22.7 (1)	42.0 (3)	4.95 (44)	0.86 (20)	5.95 (17)	1.31 (15)	0.87	100.8
88	ol	22	0.01 (1)	48.3 (2)	0.22 (3)	40.6 (2)	0.29 (2)	0.02 (1)	10.5 (2)	0.11 (5)	0.89	100.0
(3.0 GPa)	opx (av.)	12	0.21 (3)	29.5 (3)	9.15 (32)	52.1 (3)	2.29 (21)	0.20 (3)	6.06 (12)	0.43 (3)	0.90	100.2
	cpx (av.)	8	0.80 (7)	23.0 (3)	8.83 (45)	51.6 (4)	9.37 (37)	0.30 (3)	5.56 (22)	0.53 (6)	0.88	100.3
	spin	2	0.02	23.1	62.0	1.00	0.09	0.27	7.94	5.60	0.84	99.6
134	ol	61	0.03 (5)	50.1 (2)	0.18 (5)	40.7 (2)	0.35 (3)	0.01 (1)	8.45 (17)	0.21 (6)	0.91	100.8
(3.0 GPa)	opx (av.)	22	0.17 (9)	31.2 (4)	6.81 (90)	53.5 (6)	2.67 (17)	0.09 (2)	5.15 (19)	0.51 (5)	0.92	100.7
	cpx (av.)	59	0.40 (11)	25.4 (19)	6.31 (152)	52.9 (12)	9.62 (146)	0.11 (7)	4.80 (39)	0.51 (9)	0.90	100.8
	cpx (rim)	9	0.40 (11)	24.9 (6)	7.51 (33)	52.1 (3)	9.63 (82)	0.14 (5)	4.80 (29)	0.56 (5)	0.90	100.8
120	ol	184	0.01 (1)	50.2 (2)	0.21 (17)	40.8 (1)	0.31 (3)	0.00 (1)	8.32 (17)	0.17 (5)	0.91	100.5
(3.0 GPa)	opx (rim)	6 (32)	0.18 (1)	31.2 (1)	7.46 (7)	53.2 (1)	2.50 (5)	0.09 (2)	4.90 (8)	0.50 (8)	0.92	100.4
	cpx (av.)	146	0.61 (7)	25.2 (14)	7.18 (94)	52.8 (13)	8.95 (95)	0.12 (6)	4.62 (25)	0.49 (9)	0.91	100.1
	cpx (rim)	8	0.60 (4)	24.7 (1)	7.44 (11)	52.7 (2)	9.41 (7)	0.13 (2)	4.54 (9)	0.47 (4)	0.91	99.9
93	ol	9	0.04 (2)	51.5 (3)	0.22 (6)	41.1 (2)	0.29 (2)	0.00 (0)	6.79 (12)	0.11 (5)	0.93	101.2
(3.0 GPa)	opx (rim)	22 (224)	0.31 (5)	32.3 (3)	6.25 (33)	54.3 (3)	2.19 (17)	0.07 (2)	4.20 (13)	0.36 (6)	0.93	100.6
142	ol	34	0.02 (2)	49.3 (1)	0.23 (3)	40.5 (2)	0.34 (2)	0.01 (1)	9.46 (15)	0.17 (5)	0.90	100.9
(3.1 GPa)	opx (av.)	8	0.08 (1)	30.8 (3)	7.86 (42)	52.6 (3)	2.59 (23)	0.12 (2)	5.46 (13)	0.43 (4)	0.91	100.5
	cpx (av.)	44	0.31 (4)	25.5 (6)	7.36 (55)	52.3 (4)	8.79 (48)	0.13 (3)	5.20 (16)	0.43 (7)	0.90	100.6
	cpx (rim)	5	0.28 (5)	24.7 (1)	7.79 (10)	52.0 (1)	9.41 (4)	0.15 (2)	5.14 (9)	0.48 (6)	0.90	100.8
144	ol	26	0.03 (2)	49.3 (2)	0.23 (4)	40.4 (2)	0.35 (2)	0.01 (1)	9.54 (20)	0.19 (5)	0.90	100.9
(3.1 GPa)	opx (av.)	24	0.11 (2)	30.8 (4)	7.42 (81)	52.8 (6)	2.56 (17)	0.10 (3)	5.63 (15)	0.58 (9)	0.91	100.0
	cpx (av.)	52	0.33 (6)	25.3 (10)	7.51 (170)	52.0 (10)	8.80 (131)	0.15 (8)	5.27 (48)	0.58 (9)	0.90	99.9
	cpx (rim)	18	0.36 (3)	24.6 (3)	7.50 (21)	52.0 (2)	9.77 (18)	0.15 (3)	5.05 (22)	0.62 (6)	0.90	100.0
	gnt	10	0.04 (1)	22.2 (1)	23.1 (28)	42.1 (2)	5.31 (11)	0.35 (4)	5.71 (16)	1.21 (14)	0.87	100.8
141	ol	35	0.00 (1)	49.4 (2)	0.20 (3)	40.7 (2)	0.34 (3)	0.03 (2)	9.25 (17)	0.13 (5)	0.91	101.0
(3.2 GPa)	opx (av.)	9	0.11 (2)	30.8 (6)	6.90 (97)	53.4 (6)	2.65 (33)	0.11 (2)	5.62 (18)	0.46 (3)	0.91	101.1
	cpx (av.)	14	0.33 (5)	25.4 (6)	6.46 (69)	53.0 (5)	9.01 (45)	0.13 (2)	5.19 (15)	0.47 (7)	0.90	100.9
	gnt	21	0.01 (2)	22.4 (4)	23.0 (2)	42.3 (2)	5.17 (21)	0.34 (5)	5.77 (26)	1.11 (11)	0.87	101.5
138	ol	83	0.02 (2)	50.3 (2)	0.19 (3)	40.8 (2)	0.32 (2)	0.01 (1)	8.26 (16)	0.14 (5)	0.92	99.9
(3.2 GPa)	opx (av.)	26	0.09 (3)	32.1 (3)	4.90 (26)	54.8 (2)	2.65 (10)	0.04 (1)	4.94 (16)	0.50 (6)	0.92	99.9
129	ol	22	0.00 (0)	49.5 (2)	0.20 (2)	40.7 (2)	0.35 (2)	0.01 (1)	9.03 (15)	0.19 (5)	0.91	98.9
(3.3 GPa)	opx (av.)	6	0.09 (2)	31.1 (2)	6.31 (53)	53.9 (5)	2.57 (9)	0.07 (1)	5.49 (10)	0.43 (7)	0.91	98.5
	cpx (av.)	56	0.39 (6)	24.9 (10)	6.69 (73)	52.9 (6)	9.41 (93)	0.12 (4)	5.10 (34)	0.49 (8)	0.90	98.8
	gnt	11	0.01 (1)	22.3 (4)	22.9 (3)	42.2 (2)	5.11 (17)	0.31 (5)	5.98 (15)	1.14 (8)	0.87	100.0

luded to above, coexist over some pressure interval, which is, as yet, poorly constrained. Furthermore, since geochemical data indicate several % melting in the presence of residual garnet, it is appropriate to determine reaction (1) over a range of degrees of melting. To achieve this, we used two bulk compositions which are related to one another by about 7% fractional melting.

3.1. MORB-Pyrolite

At 2.7 GPa MORB-Pyrolite has a subsolidus assemblage of olivine, orthopyroxene, clinopyroxene and spinel and a solidus temperature of approximately 1450ºC. The latter is estimated from the fact that experiment 121 (Table 2) contained a trace amount (<2%) of quenched liquid. Since the solidus of Tinaquillo Lherzolite is approximately 50º higher than that of MORB-Pyrolite (Table 2) and its bulk composition is connected to the latter by about 7% melting, the ≪2% melting of experiment 121 corresponds to ≪14º above the solidus, which is within experimental uncertainty. Thus, experiment 121 at 2.7 GPa/1448º was, within uncertainty, at the MORB-Pyrolite solidus. Garnet, which is notoriously difficult to nucleate [14] appears in the oxide starting material run with small amounts of melt at 2.8 GPa and 1478ºC (exp. 122). At 2.7 GPa and 1483ºC, however, a garnet-seeded experiment (exp. 140) resulted in complete breakdown of the garnet. This demonstrates that garnet disappears close to the solidus of fertile peridotite at between 2.7 and 2.8 GPa.

The width of the field of coexistence of garnet and spinel is difficult to determine because at 2.8 and 3.0 GPa fine-grained spinel was always found armoured by olivine or orthopyroxene. We have not, however, seen evidence of stable coexistence of spinel and garnet in the experimental products. Given our experimental precision of ±15º and ±0.05 GPa the field of coexistence of the two phases must be no more than 0.1–0.2 GPa wide.

3.2. Tinaquillo Lherzolite

The more refractory nature of this composition, lower Na_2O content and higher Mg# mean that the solidus is moved to higher temperatures, and the minimum depth at which garnet is a stable near-solidus phase increases (see Fig. 1).

At 3.1 GPa and 1521ºC, two similar experiments were performed on a Tinaquillo Lherzolite composition to which about 1wt% of garnet peridotite seeds had been added. One experiment (142) produced a garnet-free spinel lherzolite assemblage, and the other (144) produced a lherzolite residue with large (80×60 μm) equant, poikilitic garnets. In each case only trace amounts of quenched melt were observed, which implies near-solidus conditions. This means that, within the experimental precision of ±0.05 GPa and ±15ºC, garnet disappears on the solidus at 3.1 GPa and 1521ºC. From the absence of spinel in direct and garnet-seeded experiments at pressures above 3.1 GPa, we deduce that the field of coexistence of garnet and spinel is about 0.1 GPa wide.

4. Discussion

Our results on the stability of garnet in natural peridotite are in excellent agreement with the work of Nickel [16] who studied the system CrCMAS (Cr_2O_3, CaO, MgO, Al_2O_3, SiO_2). If, for example, his data for a composition similar to MORB-Pyrolite, with Cr# ($= 100{*}Cr_2O_3/Cr_2O_3 + Al_2O_3$) of 9.5, are extrapolated (slope = 570ºC GPa^{-1}) to the MORB-Pyrolite solidus, a pressure of 2.84 GPa is obtained for the low-pressure disappearance of garnet. We obtain 2.8 GPa. The width of the field of coexistence of garnet and spinel obtained by Nickel is identical to our 0.1–0.2 GPa.

Most earlier results indicate, in good agreement with our data, that the garnet–spinel transition occurs between 2.5 and 3.0 GPa at temperatures close

Notes to Table 3

Analyses have been normalised to 100% for convenience with the *original* microprobe total given in the last column.

[a] (av.) is the average of all stoichiometric analyses for that phase in the experiment; (rim) is a subset of the total analyses (see [21] for a discussion on the determination of rim compositions).

[b] Number of analyses of each phase. Where orthopyroxene analyses are presented as $xx(xx)$, the analysis given is a rim composition and the number of analyses for that rim composition are a subset of the total number of analyses shown in the brackets.

Numbers in parentheses next to each analysis are 1σ in terms of the last units cited. Thus 48.8 (2) should be read as 48.8 ± 0.2.

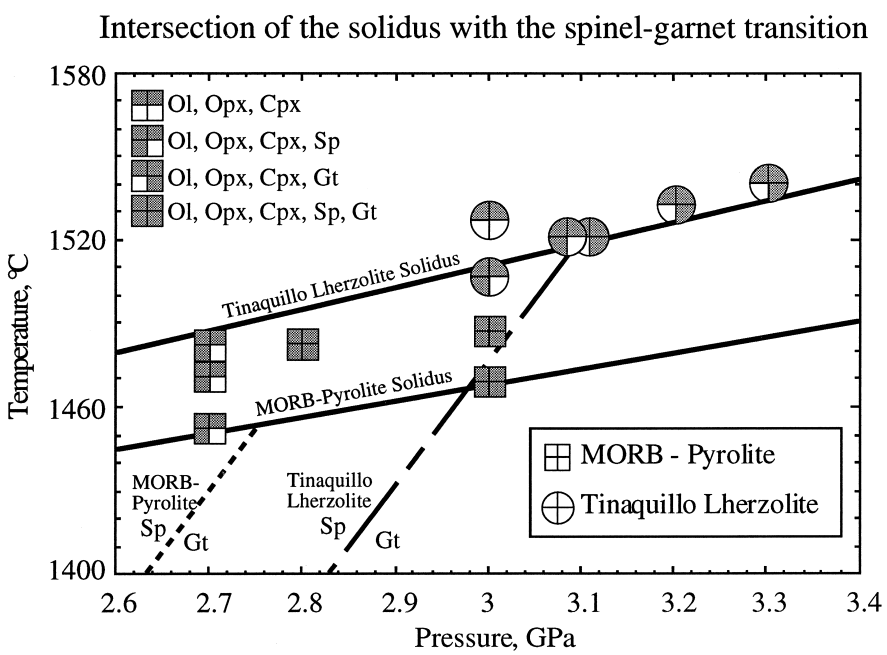

Fig. 1. Positions of the solidi (solid lines) and the spinel–garnet reaction boundaries (dashed lines) for MORB-Pyrolite and Tinaquillo Lherzolite. The P–T gradient of the spinel–garnet reaction boundary is from [16].

to the peridotite solidus [9–13,27]. An exception are the results of Kinzler [28] who found garnet appearance at 1.9–2.3 GPa in a range of basalt–peridotite mixtures. The differences appear to be due to the fact that Kinzler used much lower Cr#'s, 0.00–3.85, than those considered typical of mantle peridotite by the other authors (e.g. 6.4–7.6 [29]). As shown by Nickel [16] an increase of 6.0 in Cr# can, at low Cr contents, destabilise garnet by 0.6–1.0 GPa, enough to explain the difference between Kinzler's results and ours.

The slope of the solidi for MORB-Pyrolite and Tinaquillo Lherzolite, shown in Figs. 1 and 2, have been fitted as straight lines with gradients (60°C GPa^{-1} and 80°C GPa^{-1}, respectively) bracketing the value obtained in [27] (70°C GPa^{-1}) for a fertile peridotite and consistent with the solidus temperatures at 1.5 GPa [21]. The solidus temperature for MORB-Pyrolite, a fertile composition, is estimated to be 1470°C ± 15° at 3.0 GPa, essentially identical to the 1485°C ± 5° determined by Walter [27] for a very similar bulk composition (KR4003)

Recent studies of the trace element and isotope contents of primitive MORB have come to the conclusion that almost all of them are partially generated in the garnet stability field [1–5]. In some cases 5% integrated melting of peridotite in the garnet stability field appears to be required [5]. Following the techniques described in [27], it can be shown that Tinaquillo Lherzolite is related to MORB-Pyrolite by approximately 7% fractional melt extraction. The data indicate (Fig. 2) that the solidus temperature (T_s) increases by about 7°C for each 1% of melt that is extracted at a given pressure and that the depth of the spinel to garnet transition deepens by 0.05 GPa for each 1% of melt extracted. The heavy dotted line in Fig. 2 corresponds to an adiabat for a potential temperature of 1450°C (from [7]). It can be seen that a total of 3% anhydrous melting in the garnet stability field requires melting to begin at 3.5 GPa and 1500°C (with T_p = 1450°C) in order to overcome the retreating spinel to garnet transition and increasing solidus temperature. A potential temperature of 1470°C is required to generate 5% melting in the garnet field. Application to MORB shows that it is extremely difficult to reconcile such high potential temperatures with the actual volumes of oceanic crust observed in normal ridge segments [19]. Potential

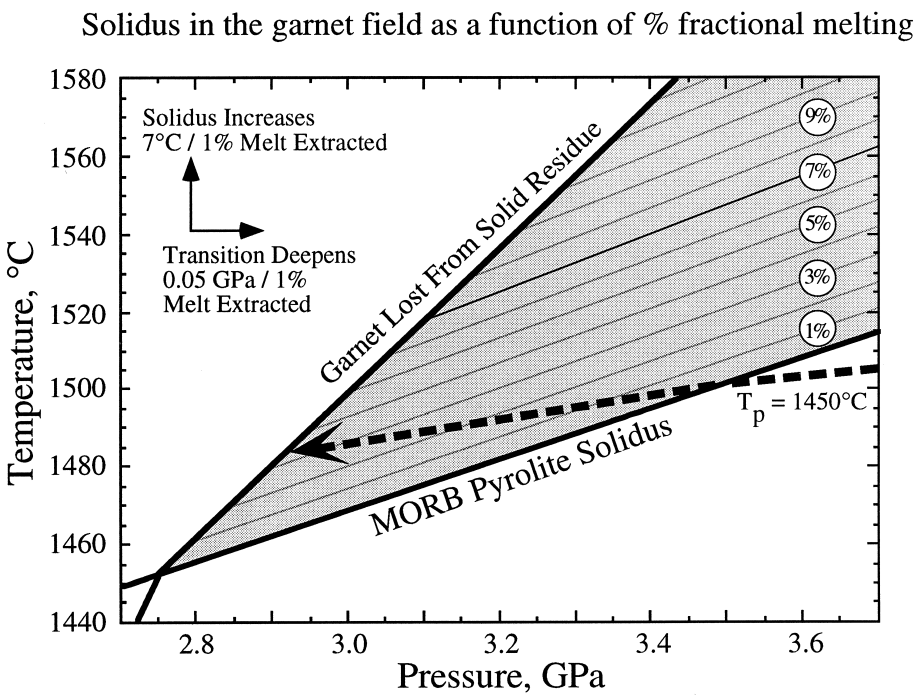

Fig. 2. The effects of partial melting on the solidus temperature and the position of the spinel–garnet reaction for fertile peridotite. Shaded area is region of near-solidus garnet stability. Initial composition is assumed to be MORB-Pyrolite and the lines labelled 1%, 3% etc. refer to the solidus for peridotite after 1% fractional melting, 3% fractional melting etc.

temperatures of 1450–1470ºC imply (based on [7]) crustal thicknesses of 14–16 km, approximately double the seismically observed range of 5–8.5 km [18].

Our data confirm, therefore, that high potential temperatures (≥1450ºC) are required to generate 3–5% anhydrous melting of garnet peridotite. If we accept that such high temperatures result in production of unreasonably large volumes of melt, then the 'garnet signature' must arise by some mechanism other than anhydrous melting of garnet peridotite [19]. Although it is beyond the scope of this paper to discuss the issue in detail, we note that several explanations have been proposed. One is that the initial melting temperature is depressed by the presence of H_2O, so that upwelling mantle at lower T_p intersects the solidus in the garnet field, giving an appropriate trace element signature with lower extents of total melting [30]. Other alternatives include partial melting of garnet pyroxenite–spinel peridotite mixtures in the spinel peridotite field [19] and a suggestion, based on high-pressure partitioning experiments, that clinopyroxene can impart the 'garnet signature' to melts within the stability field of spinel peridotite [20].

5. Conclusions

Our experiments demonstrate that the minimum pressure at which garnet is stable on the anhydrous solidus of fertile peridotite is 2.8 GPa, corresponding to a depth of about 85 km. The spinel to garnet transition, which is 0.1–0.2 GPa wide, deepens as melt is extracted from the solid residue and solidus temperatures increase. The implication is that high mantle potential temperatures (T_p > 1450ºC) are required for the 3% melting in the garnet field implied by isotopic and trace element data [1–6]. Calculated volumes of partial melt produced by upwelling mantle with such potential temperatures are approximately double those observed. This supports arguments that the 'garnet signature' in MORB is produced by some mechanism other than anhydrous melting of garnet peridotite.

Acknowledgements

This research was supported by NERC grant GR3/08730. We acknowledge the help and advice of our colleagues Jon Blundy, James Brodie, Stuart Kearns, Fred Wheeler and Mike Dury. Constructive reviews by Marc Hirschmann and Peter Ulmer assisted in revision of the manuscript. ***[FA]***

References

[1] V.J.M. Salters, S.R. Hart, The hafnium paradox and the role of garnet in the source of mid-ocean ridge basalts, Nature 342 (1989) 420–422.

[2] T.Z. La Tourette, A.K. Kennedy, G.J. Wasserburg, Thorium–uranium fractionation by garnet: evidence for a deep source and rapid rise of oceanic basalts, Science 261 (1993) 739–742.

[3] Y. Shen, D.W. Forsyth, Geochemical constraints on initial and final depth of melting beneath mid-ocean ridges, J. Geophys. Res. 100 (1995) 2211–2237.

[4] B. Bourdon, A. Zindler, T. Elliott, C.H. Langmuir, Constraints on mantle melting at mid-ocean ridges from global ^{238}U–^{230}Th disequilibrium data, Nature 384 (1996) 231–235.

[5] V.J.M. Salters, The generation of mid-ocean ridge basalts from the Hf and Nd perspective, Earth Planet. Sci. Lett. 141 (1996) 109–123.

[6] P. Beattie, The generation of uranium series disequilibria by partial melting of spinel peridotite: constraints from partitioning studies, Earth Planet. Sci. Lett. 117 (1993) 379–391.

[7] H. Iwamori, D. McKenzie, E. Takahashi, Melt generation by isentropic mantle upwelling, Earth Planet. Sci. Lett. 134 (1995) 253–266.

[8] D. McKenzie, The generation and compaction of partially molten rock, J. Petrol. 25 (1984) 713–765.

[9] D.H. Green, A.E. Ringwood, The stability fields of aluminous pyroxene peridotite and garnet peridotite and their relevance in upper mantle structure, Earth Planet. Sci. Lett. 3 (1967) 151–160.

[10] E. Takahashi, Melting of a dry peridotite KLB-1 up to 14 GPa: implications on the origin of peridotitic upper mantle, J. Geophys. Res. 91 (1986) 9367–9382.

[11] E. Takahashi, I. Kushiro, Melting of a dry peridotite at high pressures and basalt magma genesis, Am. Mineral. 68 (1983) 859–879.

[12] K. Hirose, I. Kushiro, Partial melting of dry peridotites at high pressures: determination of melts segregated using aggregates of diamonds, Earth Planet. Sci. Lett. 114 (1993) 477–489.

[13] E. Takahashi, T. Shimizaki, Y. Tsuzaki, H. Yoshida, Melting study of a peridotite KLB-1 to 6.5 GPa, and the origin of basaltic magmas, Philos. Trans. R. Soc. London 342 (1993) 105–120.

[14] D.M. Jenkins, R.C. Newton, Experimental determination of the spinel peridotite to garnet peridotite inversion at 900ºC and 1,000ºC in the system $CaO–MgO–Al_2O_3–SiO_2$, and at 900ºC with natural garnet and olivine, Contrib. Mineral. Petrol. 68 (1979) 407–419.

[15] H.S.C. O'Neill, The transition between spinel lherzolite and garnet lherzolite and its uses as a geobarometer, Contrib. Mineral. Petrol. 77 (1981) 185–194.

[16] K.G. Nickel, Phase equilibria in the system $SiO_2–MgO–Al_2O_3–CaO–Cr_2O_3$ (SMACCR) and their bearing on spinel/garnet lherzolite relationships, Neues Jahrb. Mineral. Abh. 155 (1986) 259–287.

[17] D. McKenzie, R.K. O'Nions, Partial melt distributions from inversion of rare earth element concentrations, J. Petrol. 32 (1991) 1021–1091.

[18] R.S. White, D. McKenzie, R.K. O'Nions, Oceanic crustal thickness from seismic measurements and rare earth element inversions, J. Geophys. Res. 97 (1992) 19683–19715.

[19] M.M. Hirschmann, E.M. Stolper, A possible role for garnet pyroxenite in the origin of the 'garnet signature' in MORB, Contrib. Mineral. Petrol. 124 (1996) 185–208.

[20] J.D. Blundy, J.A.C. Robinson, B.J. Wood, Heavy REE are compatible in clinopyroxene on the spinel lherzolite solidus, Earth Planet. Sci. Lett. 160 (1998) 493–504.

[21] J.A.C. Robinson, B.J. Wood, J.D. Blundy, The beginning of melting of fertile and depleted peridotite at 1.5 GPa, Earth Planet. Sci. Lett. 155 (1998) 97–111.

[22] W. Johannes, P.M. Bell, A.L. Boettcher, D.W. Chipman, J.F. Hays, H.K. Mao, R.C. Newton, F. Seifert, An interlaboratory comparison of piston-cylinder pressure calibration using the albite-breakdown reaction, Contrib. Mineral. Petrol. 32 (1971) 24–38.

[23] J. Akella, G.C. Kennedy, Melting of gold, silver and copper; proposal for a new high-pressure calibration scale, J. Geophys. Res. 76 (1971) 4969–4977.

[24] T.J.B. Holland, The reaction albite = jadeite + quartz determined experimentally in the range 600–1200ºC, Am. Mineral. 65 (1980) 129–134.

[25] A.L. Jaques, D.H. Green, Anhydrous melting of peridotite at 0–15 kb pressure and the genesis of tholeiitic basalts, Contrib. Mineral. Petrol. 73 (1980) 287–310.

[26] L.E. Wasylenki, M.B. Baker, M.M. Hirschmann, E.M. Stolper, The effect of source depletion on equilibrium mantle melting, Eos 77 (1996) F847.

[27] M.J. Walter, Melting of garnet peridotite and the origin of komatiite and depleted lithosphere, J. Petrol. 39 (1998) 29–60.

[28] R.J. Kinzler, Melting of mantle peridotite at pressures approaching the spinel to garnet transition: application to mid-ocean ridge basalt petrogenesis, J. Geophys. Res. 102 (1997) 853–874.

[29] T.J. Falloon, D.H. Green, Anhydrous partial melting of MORB Pyrolite and other peridotite compositions at 10 kbar: implications for the origin of primitive MORB glasses, Mineral. Petrol. 37 (1987) 181–219.

[30] G. Hirth, D.L. Kohlstedt, Water in the oceanic upper mantle: implications for rheology, melt extraction and the evolution of the lithosphere, Earth Planet. Sci. Lett. 144 (1996) 93–108.